Structures, Electronic Properties, and Oxidation−Reduction Reactivity of Halogenated Iron Porphyrins

Mark W. Grinstaff, Michael G. Hill,† Eva R. Birnbaum, William P. Schaefer, Jay A. Labinger,* and Harry B. Gray*

Arthur Amos Noyes Laboratory, California Institute of Technology, Pasadena, California 91125

Received January 27, 1995[⊗]

Molecular structures of both $Fe^{III}(TFPPBr_8)Cl$ and $Fe^{II}(TFPPBr_8)(py)_2$ porphyrins reveal saddle distortions: $Fe^{III}(TFPPBr_8)Cl$ in triclinic space group $P\bar{1}$, $a = 13.649(4)$ Å, $b = 14.474(4)$ Å, $c = 14.537$ Å, $\alpha = 89.26(2)°$, $\beta = 67.13(1)°$, $\gamma = 71.82(2)°$, $V = 2494.3(13)$ Å^3, $Z = 2$; $Fe^{II}(TFPPBr_8)(py)_2$ in triclinic space group $P\bar{1}$, $a = 12.459(7)$ Å, $b = 13.125(8)$ Å, $c = 20.989(11)$ Å, $\alpha = 84.72(5)°$, $\beta = 72.87(4)°$, $\gamma = 69.04(5)°$, $V = 3063(3)$ Å^3, $Z = 2$. Similar to other chloro−iron(III) porphyrins, μ_{eff} at room temperature (5.96 μ_B) is that of a $^6A_1$ state; μ_{eff} at 2 K (4.2 μ_B) indicates a large zero-field splitting. The Soret bands of both $Fe^{III}(TFPPBr_8)Cl$ and $Fe^{II}(TFPPBr_8)(py)_2$ are red-shifted by approximately 23 nm relative to those of corresponding planar Fe^{III} porphyrins. The metal and porphyrin reduction potentials of $Fe^{III}(TFPPBr_8)Cl$ and $Fe^{II}(TFPPBr_8)(py)_2$ are anodically shifted more than 400 mV from those of $Fe^{III}(TPP)Cl$. Although $[Fe^{II}(TFPPBr_8)Cl]^-$ reacts very slowly with dioxygen, it is oxidized rapidly by *tert*-butyl hydroperoxide (TBHP); these Fe^{II} reactivity properties taken together with the finding that the corresponding Fe^{III} complex is reduced rapidly by TBHP provide strong support for the proposal that $Fe^{III}(TFPPBr_8)Cl/O_2$-catalyzed alkane oxygenations occur by a radical chain mechanism in which alkyl hydroperoxide intermediates are decomposed efficiently by both Fe^{III} and Fe^{II} species.

Introduction

Perhalogenated metalloporphyrins[1] are robust catalysts for alkane hydroxylation by dioxygen at relatively low temperatures and pressures.[2,3] Among the several pathways that could lead to hydroxylation, Lyons and Ellis favored one involving an iron(IV)−oxo as the active oxygenating species.[2] This mechanism is related to that proposed for cytochrome P450,[4] except that the iron−oxo, $(TFPPX_8)Fe^{IV}=O$, is formed by homolysis of a peroxo-bridged iron(III) dimer (*i.e.*, $Fe^{III}-O-O-Fe^{III}$). Unlike P450, then, the $Fe^{II}(TFPPX_8)/O_2$ system does not need a coreductant for catalytic activity. Both pathways, however, require dioxygen binding to iron(II) prior to iron−oxo formation.

The iron(III/II) reduction potential of $Fe^{III}(TFPPBr_8)Cl$ is roughly 0.6 V higher than that of $Fe^{III}(TPP)Cl$, and spectroelectrochemical experiments have shown that $Fe^{II}(TFPPBr_8)$ is kinetically stable in the presence of dioxygen.[5] We have suggested, therefore, that $Fe^{III}(TFPPBr_8)Cl/O_2$-catalyzed alkane oxygenations occur by a mechanism featuring Fe^{III} oxidation and Fe^{II} reduction of alkyl hydroperoxides to generate alkoxy and peroxy radicals that subsequently combine to produce an alcohol.[5,6]

Since it would be of special interest if the iron(III/II) electronic states played a specific role in the electron-transfer reactivity of these molecules, we would like to know whether the highly distorted geometries of perhalogenated porphyrins are associated with unusual $Fe^{III/II}$ electronic structures. Therefore, we have investigated the spectroscopic, magnetic, and electrochemical properties of two structurally characterized $TFPPBr_8$ complexes, $Fe^{III}(TFPPBr_8)Cl$ and $Fe^{II}(TFPPBr_8)(py)_2$.

Results and Discussion

Structural Motifs. ORTEP drawings of $Fe^{III}(TFPPBr_8)Cl$ and $Fe^{II}(TFPPBr_8)(py)_2$ are shown in Figures 1 and 2; crystal data and selected bond distances and angles are set out in Tables 1−3.[7] Both complexes have twisted S_4 saddle-shaped structures, as reflected in the displacement of the pyrrole-edge carbon atoms

† Current address: Department of Chemistry, Occidental College, Los Angeles, California 90046

⊗ Abstract published in *Advance ACS Abstracts,* August 1, 1995.

(1) Abbreviations for porphyrin dianions: TPP = 5,10,15,20-tetraphenylporphyrin; TFPP = tetrakis(5,10,15,20-pentafluorophenyl)porphyrin; $TFPPBr_8$ = 2,3,7,8,12,13,17,18-octabromo-5,10,15,20-tetrakis(pentafluorophenyl)porphyrin; $TFPPCl_8$ = 2,3,7,8,12,13,17,18-octachloro-5,10,15,20-tetrakis(pentafluorophenyl)porphyrin; $TPP(CH_3)_8$ = 2,3,7,8,12,13,17,18-octamethyl-5,10,15,20-tetraphenylporphyrin; $TPP(C_2H_5)_8$ = 2,3,7,8,12,13,17,18-octaethyl-5,10,15,20-tetraphenylporphyrin.

(2) (a) Ellis, P. E.; Lyons, J. E. *Catal. Lett.* **1989**, *3*, 389−398. (b) Ellis, P. E.; Lyons, J. E. *Coord. Chem. Rev.* **1990**, *105*, 181−193. (c) Lyons, J. E.; Ellis, P. E. *Catal. Lett.* **1991**, *8*, 45−51. (d) Lyons, J. E.; Ellis, P. E.; Wagner, R. W.; Thompson, P. B.; Gray, H. B.; Hughes, M. E.; Hodge, J. A. *Proceedings of the Am. Chem. Soc. Div. of Petroleum Chemistry, Symposium on Natural Gas Upgrading II;* American Chemical Society: Washington, DC, 1992, pp 307−317.

(3) Catalytic oxidation by metalloporphyrins (using oxidants other than O_2) is often enhanced by halogenation of the porphyrin macrocycle: (a) Bartoli, J. F.; Brigaud, O.; Battioni, P.; Mansuy, D. *J. Chem. Soc., Chem. Commun.* **1991**, 440−442. (b) Traylor, T. G.; Hill, K. W.; Fann, W.; Tsuchiya, S.; Dunlap, B. E. *J. Am. Chem. Soc.* **1992**, *114*, 1308−1312. (c) Bruice, T. C.; He, G. *J. Am. Chem. Soc.* **1991**, *113*, 2747−2753. (d) Wijesekera, T.; Matsumoto, A.; Dolphin, D.; Lexa, D. *Angew. Chem., Int. Ed. Engl.* **1990**, *29*, 1028−1030. (e) Ellis, P. E.; Lyons, J. E. *J. Chem. Soc., Chem. Commun.* **1989**, 1315−1316. (f) Ostovic, D.; Knobler, C. B.; Bruice, T. C. *J. Am. Chem. Soc.* **1987**, *109*, 3444−3451. (g) Traylor, T. G.; Tsuchiya, S.; Byun, Y.; Kim, C. *Inorg. Chem.* **1987**, *26*, 1338−1339. (h) Chang, C. K.; Ebina, F. *J. Chem. Soc., Chem. Commun.* **1981**, 778−779. (i) Recent reviews on metalloporphyrin chemistry/catalysis: Mansuy, D. *Coord. Chem. Rev.* **1993**, *125*, 129−141 and Meunier, B. *Chem Rev.* **1992**, *92*, 1411−1456.

(4) Ortiz de Montellano, P. *Cytochrome P-450: Structure, Mechanism, and Biochemistry*; Plenum: New York, 1986.

(5) Grinstaff, M. W.; Hill, M. G.; Labinger, J. A.; Gray, H. B. *Science* **1994**, 264, 1311−1313.

(6) Labinger, J. A. *Catal. Lett.* **1994**, *26*, 95−99.

(7) Two crystal structures of halogenated iron porphyrins have been reported: $[Fe(TFPP)]_2O$ (Gold, A.; Jayaraj, K.; Doppelt, P.; Fischer, J.; Weiss, R. *Inorg. Chim. Acta* **1988**, *150*, 177−181) and $Fe(TCl_4PP)(NNC_9H_{18})$ (Mahy, J. P.; Battioni, P.; Mansuy, D.; Fisher, J.; Weiss, R.; Mispelter, J.; Morgenstern-Badarau, I.; Gans, P. *J. Am. Chem. Soc.* **1984**, *106*, 1699−1706).

0020-1669/95/1334-4896$09.00/0

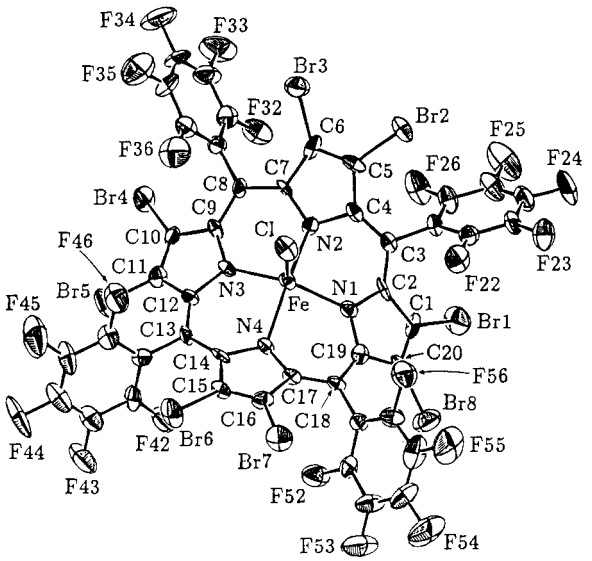

Figure 1. ORTEP diagram of $Fe^{III}(TFPPBr_8)Cl$ with ellipsoids drawn at the 50% probability level.

(and bromine atoms) from the least-squares plane (Table 4). Furthermore, the steric repulsion between adjacent bromine atoms creates deviations from the ideal dihedral plane (*e.g.*, Br1−C1−C20−Br8; 3.1° in $Fe^{III}(TFPPBr_8)Cl$). The magnitude of the porphyrin distortion in these five-and six-coordinate iron complexes is similar to that in four-coordinate metallo analogs (Table 4) such as $Ni(TFPPBr_8)$,[8] $Cu(TFPPCl_8)$,[9] $Zn(TFPPBr_8)$,[10] $Cu(TFPPBr_8)$,[11] $Zn(TPP(CH_3)_8)$,[12] and $Zn(TPP(C_2H_5)_8)$.[12] The distortion of the porphyrin in $Ru(TFPPCl_8)(CO)(H_2O)$ also is similar.[13]

The porphyrin central cores of both $Fe^{III}(TPP)Cl$ and $Fe^{III}(TFPPBr_8)Cl$ are similar in that their bond lengths are comparable (*i.e.*, less than 0.04 Å difference), and the iron is displaced from the N_4 plane in both porphyrins by approximately 0.49 Å.[14,15] However, the core geometries of the two porphyrins are quite different. In $Fe^{III}(TPP)Cl$ the N−Fe−Cl bond angles vary only from 103 to 104.7°, whereas in $Fe^{III}(TFPPBr_8)Cl$ the bond angles range from 98.6 to 108.8° as a consequence of macrocyclic S_4 distortion. The N−Fe−N angles also deviate from those of square pyramidal Fe(TPP)Cl with the N1−Fe−N3 and N2−Fe−N4 angles being larger and smaller by approximately 5°, respectively, resulting in a rhombohedral distortion about the iron. The central core of $Fe^{II}(TFPPBr_8)(py)_2$ is dramatically different due to the addition of a second axial ligand; the iron lies in the plane of the four nitrogen atoms with the pyridine ligands staggered approximately 90° to each other.

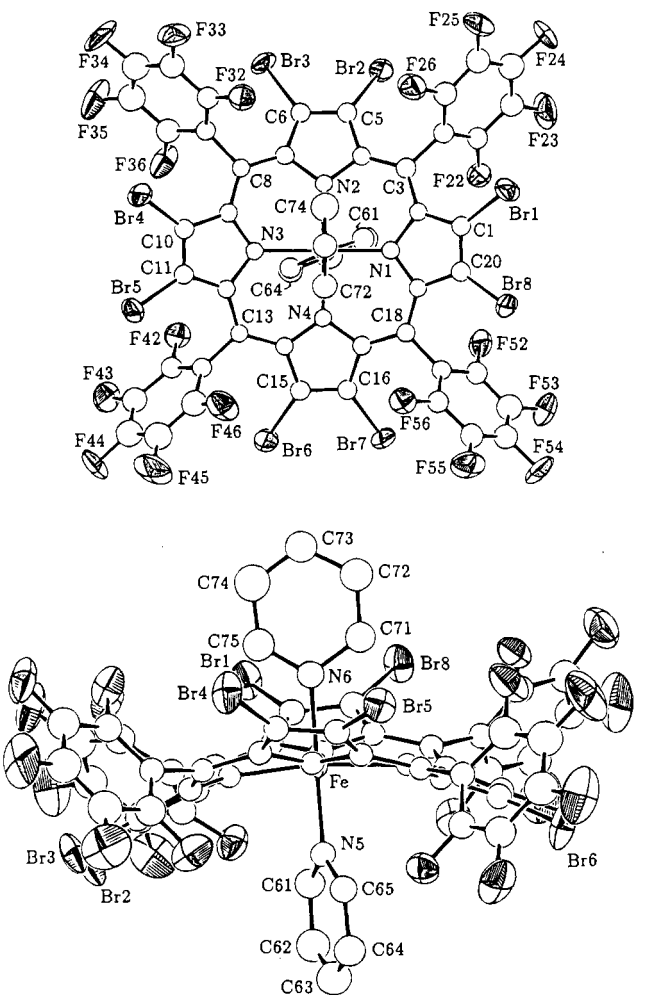

Figure 2. ORTEP diagrams of $Fe^{II}(TFPPBr_8)(py)_2$ with ellipsoids drawn at the 50% probability level.

Magnetic Properties. The frozen-glass EPR spectrum of $Fe^{III}(TFPPBr_8)Cl$ at 4.3 K reveals a highly rhombic iron−porphyrin ground state (Figure 3A). Both the $S = {}^5/_2$ and $S = {}^3/_2$ states are populated at 4.3 K (g = 6.7, 5.2, 4.4, 3.8, and 1.9). Although signals due to $S = {}^5/_2$ states of $Fe^{III}(TFPP)Cl$ and $Fe^{III}(TPP)Cl$ are observed at 77 K ($g_\perp$= 6 and $g_\parallel$ = 2), $Fe^{III}(TFPPBr_8)Cl$ is EPR silent above 15 K.[16] Magnetic susceptibility measurements from 2 to 300 K give a μ_{eff} (300 K) of 5.96 μ_B, very close to the spin-only value for a $^6A_1$ state (5.92 μ_B) (Figure 3B). The μ_{eff} is constant from about 50 to 300 K, and its value is similar to that of other five-coordinate iron(III) porphyrins with axial halides.[17] The μ_{eff} value drops rapidly below 50 K, indicating a large zero-field splitting ($D \gg h\nu$); by 2 K the μ_{eff} is 4.2 μ_B. The EPR pattern from 1500 to 2500 G is characteristic of a rhombic $S = {}^3/_2$ state with an average g of roughly 4.1; this spin-state assignment is further supported by a Brillouin fit at 2 K of the magnetization versus $H(G)/T(K)$ that yields S = 1.68.

Visible Spectroscopy and Electrochemistry. Halogenation of the porphyrin macrocycle at the β-pyrrole position shifts the Soret absorption to lower energy (Table 5). In the spectrum of

(8) (a) Mandon, D.; Ochsenbein, P.; Fischer, J.; Weiss, R.; Jayaraj, K.; Austin, R. N.; Gold, A.; White, P. S.; Brigaud, O.; Battioni, Mansuy, D. *Inorg. Chem.* **1992**, *31*, 2044−2049.
(9) Schaefer, W. P.; Hodge, J. A., Hughes, M. E; Gray, H. B.; Lyons, J. E.; Ellis, P. E.; Wagner, R. W. *Acta Crystallogr.* **1993**, *C49*, 1342−1345.
(10) Marsh, R. E.; Schaefer, W. P.; Hodge, J. A.; Hughes, M. E.; Gray, H. B. *Acta Crystallogr.* **1993**, *C49*, 1339−1342.
(11) Henling, L. M.; Schaefer, W. P.; Hodge, J. A.; Hughes, M. E.; Gray, H. B. *Acta Crystallogr.* **1993**, *C49*, 1743−1747.
(12) Barkigia, K. M.; Berber, M. D.; Fajer, J.; Medford, C. J.; Renner, M. W.; Smith, K. M. *J. Am. Chem. Soc.* **1990**, *112*, 8851−8857.
(13) Birnbaum, E. R.; Schaefer, W. P.; Labinger, J. A.; Bercaw, J. E.; Gray, H. B. *Inorg. Chem.* **1995**, *34*, 1751−1755.
(14) Crystal structure of Fe(TPP)Cl: Scheidt, W. R.; Finnegan, M. G. *Acta Crystallogr.* **1989**, *C45*, 1216−1218. The structure of Fe(TFPP)Cl has not been determined.
(15) The structures of Zn(TPP) (Scheidt, W. R.; Kastner, M. E.; Hatano, K. *Inorg. Chem.* **1978**, *17*, 706−710) and Zn(TFPP) (ref 7) are similar in almost all respects (*i.e.*, analogous distances and angles, as well as ring planarity).
(16) (a) One example of a $S = {}^3/_2$ iron porphyrin [Fe(TPP)[C=C(*p*-$ClC_6H_4)_2$](Cl) has been reported: Mansuy, D.; Morgenstern-Badarau, I.; Lange, M.; Gans, P. *Inorg. Chem.* **1982**, *21*, 1427−1430. (b) The EPR spectrum of Fe(TPP)Cl has been reported: Sato, M.; Rispin, A. S.; Kon, H. *Chem. Phys.* **1976**, *18*, 211.
(17) (a) Behere, D. V.; Mitra, S. *Ind. J. Chem.* **1980**, *19A*, 505−507. (b) Mitra, S. In *Iron Porphyrins Part II*, Lever, A. B. P., Gray, H. B., Eds.; Addison-Wesley Publishing: London, 1983: pp 1−42.

Table 1. Crystallographic and Refinement Data for $Fe^{III}(TFPPBr_8)Cl$ and $Fe^{II}(TFPPBr_8)(py)_2$

X-ray Parameters	$Fe^{III}(TFPPBr_8)Cl$	$Fe^{II}(TFPPBr_8)(py)_2$
formula	$C_{44}Br_8ClF_{20}FeN_4$	$C_{44}H_{15}Br_8F_{20}FeN_7$
M_R	1695.01	1896.86
color	black	dark red
shape	irregular chunk	skewed parallelepiped
crystal system	triclinic	triclinic
space group	$P\bar{1}$	$P\bar{1}$
a, Å	13.649(4)	12.459(7)
b, Å	14.474(4)	13.125(8)
c, Å	14.537(4)	20.989(11)
α, deg	89.26(2)	84.72(5)
β, deg	67.13(2)	72.87(4)
γ, deg	71.82(2)	69.04(5)
V, Å^3	2494.3(13)	3063(3)
Z	2	2
D_x, g cm^{-3}	2.26	2.06
radiation	Mo Kα	Mo Kα
wavelength, Å	0.710 73	0.710 73
μ, cm^{-1}	68.15	55.20
temp, K	296	297
cryst size, mm	0.12 × 0.19 × 0.22	0.18 × 0.26 × 0.35
diffractometer	Enrad-Nonius Cad-4	Enrad-Nonius Cad-4
collcn method	ω scans	ω scans
θ range, deg	1−20	1−20
$h_{min/max}$	−13/13	−11/11
$k_{min/max}$	−13/13	−12/12
$l_{min/max}$	−14/14	−20/20
reflcns measd	9596	11 801
indepdt reflcns	4630	5673
reflcns used	4630	5673
R_{int}	0.029	0.045
$R(F)$	0.075	0.071
$R_w(F^2)$	0.011	0.005
goodness of fit	2.47	1.30

Table 2. Selected Bond Lengths (Å) for $Fe^{III}(TFPPBr_8)Cl$ and $Fe^{II}(TFPPBr_8)(py)_2$

bond	$Fe^{III}(TFPPBr_8)Cl$	$Fe^{II}(TFPPBr_8)(py)_2$
Fe−Cl	2.191(4)	
Fe−Npy		2.012(7)
Fe−N1	2.062(11)	1.963(7)
Fe−N2	2.066(11)	1.958(7)
Fe−N3	2.039(11)	1.968(7)
Fe−N4	2.054(11)	1.964(7)
N1−C2	1.391(18)	1.384(11)
C2−C3	1.39(2)	1.400(12)
C2−C1	1.44(2)	1.454(12)
C1−C20	1.35(2)	1.329(12)
C1−Br1	1.891(15)	1.856(9)

$Fe^{III}(TFPPBr_8)Cl$, the Soret absorption (440 nm) is red-shifted by approximately 23 nm compared to those of $Fe^{III}(TPP)Cl$ (416 nm) and $Fe^{III}(TFPP)Cl$ (418 nm). Semiempirical (AM1) electronic structure calculations indicate that the similar bathochromic shifts for $Zn(TFPPBr_8)$ and $Zn(TPP(C_2H_5)_8)$ are a consequence of macrocyclic distortion.[18] These calculations suggest that the frontier orbitals are destabilized by the distortion; but the LUMO is destabilized to a lesser extent than the HOMO, resulting in red-shifted Soret bands. The electronegativity of the halogen substituents also influences the electrochemical properties.[19] The perhalogenated iron porphyrin ring-centered oxidations and reductions are anodically shifted compared to Fe(TPP)Cl (Table 5). In contrast, a cathodic shift

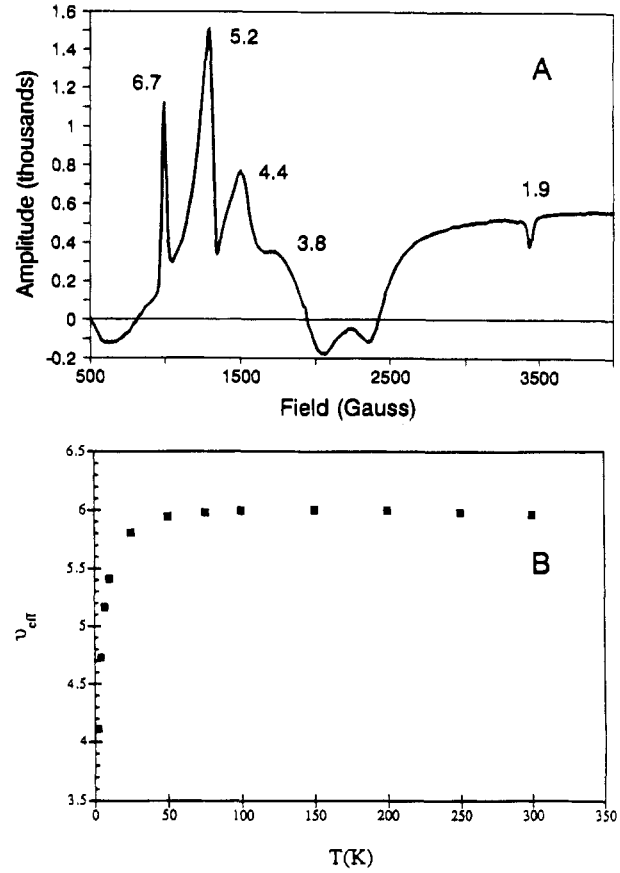

Figure 3. (A) EPR spectrum of $Fe^{III}(TFPPBr_8)Cl$ (toluene glass, 4.3 K). (B) Plot of μ_{eff} (μ_B) *vs* T (K) for $Fe^{III}(TFPPBr_8)Cl$ (2−300 K; 10 kG).

Table 3. Selected Angles (deg) for $Fe^{III}(TFPPBr_8)Cl$ and $Fe^{II}(TFPPBr_8)(py)_2$

angle	$Fe^{III}(TFPPBr_8)Cl$	$Fe^{II}(TFPPBr_8)(py)_2$
N1−Fe−Cl	108.8(3)	
N2−Fe−Cl	98.6(3)	
N1−Fe−N5py		93.0(3)
N2−Fe−N6py		85.1(3)
N1−Fe−N2	87.1(4)	90.3(3)
N1−Fe−N3	146.6(4)	170.9(3)
N2−Fe−N3	86.8(4)	90.3(3)
N1−C2−C3	122.5(13)	122.2(8)
N1−C2−C1	106.4(12)	109.0(7)
C2−C1−C20	110.7(13)	108.1(8)
C2−C1−Br1	123.9(11)	128.4(7)

in the ring-centered oxidations and reductions is observed for complexes such as $Zn(TPP(CH_3)_8)$[12] that contain electron-donor substitutents. Replacement of the phenyl group (*i.e.*, TPP) at the meso position with a perfluorophenyl moiety (*i.e.*, TFPP) anodically shifts the $E_{ox}(0/+1)$ potential by 510 mV (Table 5). Subsequent bromination of the pyrrole positions further shifts the potential by at least another 150 mV. As with the HOMO, the LUMO is dramatically stabilized by introducing halogens in the macrocycle. E_{red} (0/−1) is 440 mV more positive for $Fe^{III}(TFPPBr_8)Cl$ than $Fe^{III}(TPP)Cl$. Consequently, increased halogenation of the porphyrin macrocycle at both the meso and β positions produces complexes that are easier to reduce and harder to oxidize.

Halogen substituents on the porphyrin macrocycle substantially affect the metal electrochemistry as well (Table 5). The

(18) (a) Takeuchi, T.; Gray, H. B.; Goddard, W. A. *J. Am. Chem. Soc.* **1994**, *116*, 9730−9732. (b) Kadish, K. M.; D'Souza, F.; Villard, A.; Autret, M.; Van Caemelbecke, E.; Bianco, P.; Antonini, A.; Tagliatest, P. *Inorg. Chem.* **1994**, *33*, 5169−5170. (c) Barkigia, K. M.; Chantranupong, L.; Smith, K. M.; Fajer, J. *J. Am. Chem. Soc.* **1988**, *110*, 7566−7567. (d) Gassman, P. G.; Ghosh, A.; Almlof, J. *J. Am. Chem. Soc.* **1992**, *114*, 9990−10000.

(19) Phillippi, M. A.; Shimomura, E. T.; Goff, H. M. *Inorg. Chem.* **1981**, *20*, 1322−1325. The $E_{ox}(0/+1)$ potential of $Fe(TFPPBr_8)Cl$ could not be measured as it was shifted beyond the CH_2Cl_2 solvent limit (1.8 V *vs* Ag/AgCl).

Table 4. Average Deviations (Å) of Atoms from Least-Squares Planes

atom	$Fe^{III}(TFPPBr_8)Cl$	$Fe^{II}(TFPPBr_8)(py)_2$	$Cu^{II}(TFPPBr_8)$	$Ni^{II}(TFPPBr_8)$
M	0.485	0.01	0.003	0.001
N	0.10	0.15	0.15	0.19
C_{meso}	0.22	0.17	0.18	0.21
C_{beta}	1.17	1.09	1.25	1.33
Br_{odd}	2.13	1.87	2.16	2.25
Br_{even}	1.81	1.58	1.86	1.86

Table 5. Spectroscopic and Electrochemical Properties of Halogenated Iron Porphyrins[a]

	$Fe^{III}(TPP)Cl$	$Fe^{III}(TFPP)Cl$	$Fe^{III}(TFPPBr_8)Cl$	$[Fe^{II}(TFPPBr_8)Cl]^-$	$Fe^{II}(TFPPBr_8)(py)_2$
g.s.	H. S. d^5	H. S. d^5	H. S. d^5		L. S. d^6
Soret (nm)	416	418	440	474	454
III/II (V)	−0.29	−0.08	0.31	0.31	0.82
0/-1 (V)	−1.07	−1.10	−0.63	−0.63	−0.75
0/+1 (V)	1.14	1.65	not obsd	not obsd	not obsd

[a] UV−vis absorption measurements in CH_2Cl_2. All potentials are reported *vs* AgCl/Ag in 1 M KCl.

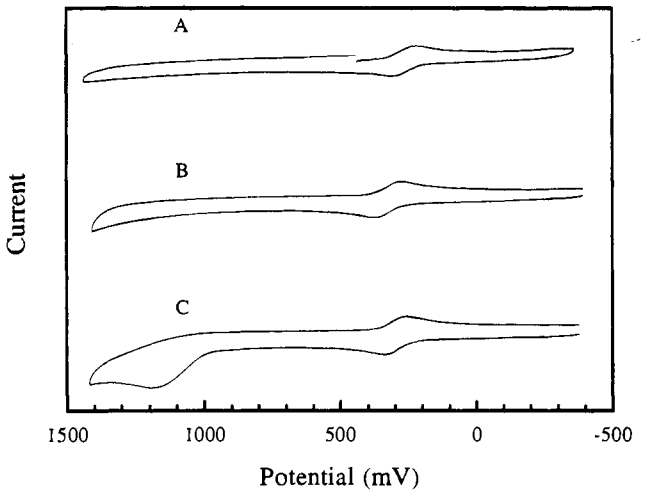

Figure 4. (A) Cyclic voltammogram of $Fe^{III}(TFPPBr_8)Cl$ in 0.1 M TBAH/CH_2Cl_2. (B) Cyclic voltammogram of the same solution after bulk electrolysis at 0.0 V. (C) Cyclic voltammogram of (B), after the addition of 1 mM TBACl. The large anodic current at approximately 1.0 V corresponds to the oxidation of chloride to chlorine. All potentials are reported *vs* AgCl/Ag in 1 M KCl.

potential of the iron(III/II) couple of $Fe^{III}(TFPPBr_8)Cl$ is 600 mV more positive than that of $Fe^{III}(TPP)Cl$. The spectroelectrochemistry of $Fe^{III}(TFPPBr_8)Cl$ reveals a clean isosbestic (457 and 580 nm) transformation between the iron(III) (402, 442, and 560 nm) and the iron(II) (478 and 598 nm) porphyrins. Interestingly, in 0.1 M TBAH/CH_2Cl_2, it appears that the iron(II) species remains five-coordinate with chloride in the axial position. Figure 4A shows the cyclic voltammogram of $Fe^{III}(TFPPBr_8)Cl$ with a reversible reduction at 0.31 V (*vs* AgCl/Ag). Bulk reduction of this solution at 0.0 V yields the iron(II) complex, which shows a reversible oxidation at 0.31 V (Figure 4B). Importantly, this bulk-reduced solution shows no wave corresponding to the oxidation of the free chloride in solution (Figure 4C), implying that the chloride is tightly bound in the iron(II) oxidation step.[20] This observation is supported by the ^{19}F NMR spectrum of the electrochemically generated iron(II) complex, $[Fe^{II}(TFPPBr_8)Cl]^-$, which is consistent with a paramagnetic, five-coordinate metal center (*i.e.*, pairs of resonances are observed for the ortho and meta fluorines; −124, −133 ortho; −148 para; −158, −160 meta). In reduction of the chlorinated analog $Fe^{III}(TPPCl_8)Cl$, it has been suggested that

Scheme 1. Key Mechanistic in the Catalytic Oxidation of Alkanes: Oxidation and Reduction of Alkyl Hydroperoxides by Perhalogenated Iron Porphyrins

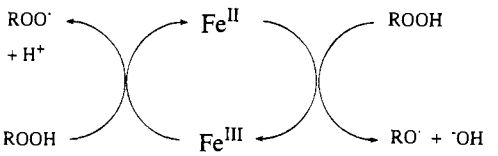

the axial chloride remains bonded to iron(II).[21] On the other hand, the NMR spectrum of chemically reduced (ascorbic acid in methanol) $Fe^{III}(TFPPBr_8)Cl$ is consistent with a diamagnetic, six-coordinate iron species, $Fe^{II}(TFPPBr_8)(HOCH_3)_2$. The addition of pyridine to $Fe^{III}(TFPPBr_8)Cl$ produces the diamagnetic $Fe^{II}(TFPPBr_8)(py)_2$ (Figure 2). This iron(II) state is further stabilized compared to $Fe^{III}(TFPPBr_8)Cl$. A reversible wave is observed in the cyclic voltammogram of $Fe^{II}(TFPPBr_8)(py)_2$ in solution; the iron(III/II) reduction potential is 0.82 V *vs* AgCl/Ag (Table 5).

Oxidation−Reduction Reactivity. The hydroxylation mechanism proposed for halogenated iron porphyrins and dioxygen involves alkyl hydroperoxide decomposition *via* single electron transfer from the iron heme (Scheme 1).[5,6] Oxidation and reduction of the alkyl hydroperoxide by the iron catalytically generates radicals that propagate the reaction *via* free-radical chemistry to form the oxidized products. As shown in Figure 7, light alkane hydroxylation catalytic activity (% consumption of isobutane to *tert*-butanol) increases as a function of porphyrin−iron(III/II) potential (*i.e.*, halogenation).[2] Halogenation of the porphyrin macrocycle promotes the oxidation−reduction of peroxides in several ways as opposed to the reaction of the iron(II) complex with dioxygen and the subsequent steps to form a reactive high-valent iron−oxo species (*i.e.*, either $Fe^{III}-O-O-Fe^{III}$ homolysis or reduction of an $Fe^{II}-O_2$ complex analogous to peroxidase chemistry).

The large saddle distortion of the $TFPPBr_8$ macrocycle originates from severe van der Waals contacts; the TFPP and TPP analogs are planar. Molecular models suggest this distorted structure favors monomers over dimers in solution. Molecular models of $[Fe^{III}(TFPPBr_8)]_2O$ show severe steric clash between adjacent porphyrin bromine−bromine and bromine−fluorine atoms in both the eclipsed (along the Fe−O−Fe axis) and staggered structures; the bulk of the ligand prohibits close contact of the two iron centers.[22] In contrast, the planar TFPP

(20) The iron(III/II) reduction potential of $Fe(TFPPBr_8)Cl$ also did not alter with electrolyte counteranion (*e.g.*, PF_6^- or ClO_4^- or Cl^-). The $[Fe^{II}(TFPPBr_8)Cl]^-$ complex is isolatable; however X-ray-quality crystals have not yet been obtained.

(21) Wijesekera, T.; Matsumoto, A.; Dolphin, D. *Angew. Chem.* **1990**, *29*, 1028−1029.

(22) Molecular models are based on the X-ray crystal coordinates of Fe(TFPPBr$_8$)Cl and Fe(TFPP)−O−Fe(TFPP) (ref. 7).

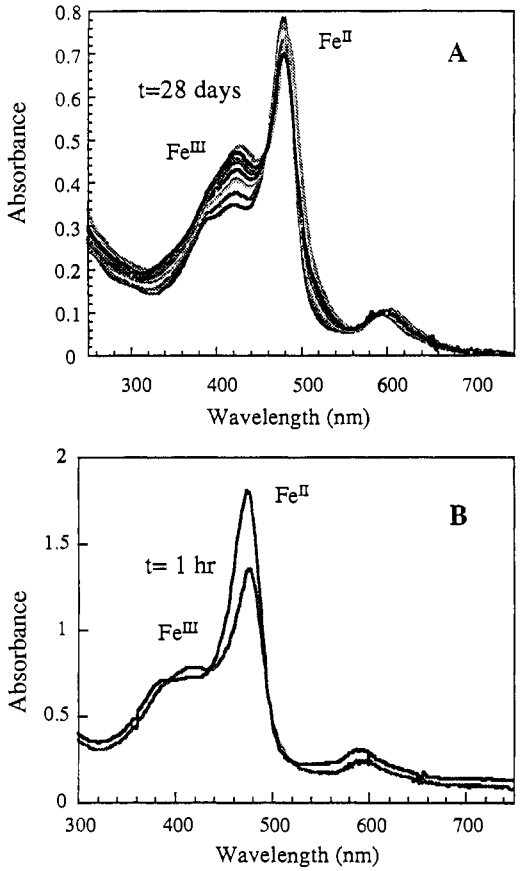

Figure 5. (A) Autoxidation of $[Fe^{II}(TFPPBr_8)Cl]^-$ (1 atm of dioxygen) in methylene chloride at 23 °C. (B) Autoxidation of $[Fe^{II}(TFPPBr_8)Cl]^-$ (3 atm of dioxygen) in toluene at 65 °C.

and TPP iron complexes form thermodynamically favored μ-oxo complexes in the presence of oxygen.[7,23] Consequently, the monomeric perhalogenated complexes are free to react with the alkyl hydroperoxide in solution even with oxygen present. Although the monomeric iron porphyrin is sterically crowded, an alkyl hydroperoxide such as *tert*-butyl hydroperoxide (TBHP) can reside in the porphyrin pocket with minimal steric constraints.[5]

Halogenation at both the meso and β-positions stabilizes the porphyrin against oxidative degradation. Ring-centered oxidation in the electrochemistry of $Fe^{III}(TFPPBr_8)Cl$ is not observed within the solvent limit (~1.8 V) of CH_2Cl_2, whereas oxidations of $Fe^{III}(TFPP)Cl$ and $Fe^{III}(TPP)Cl$ occur at 1.50 and 1.30 V. Further, there are no carbon–hydrogen bonds to be oxidatively cleaved as in TFPP and TPP. Thus, $Fe^{III}(TFPPBr_8)Cl$ can remain catalytically active in a highly oxidizing environment.

Importantly, the anodically shifted iron(III/II) potential of $Fe^{III}(TFPPBr_8)Cl$ relative to those of the TFPP and TPP analogs alters the reaction pathway. Unlike most iron(II) porphyrins, the $[Fe^{II}(TFPPBr_8)Cl]^-$ complex is kinetically stable in the presence of dioxygen: electrochemically generated solutions of $[Fe^{II}(TFPPBr_8)Cl]^-$ autoxidize very slowly (days) at 1 atm O_2 and 23 °C. Even at moderately elevated pressure and temperature (3 atm of O_2 and 65 °C), there is less than ~15% autoxidization in 1 h (Figure 5). In contrast, both $Fe^{II}(TFPP)$ and $Fe^{II}(TPP)$ autoxidize rapidly in the presence of dioxygen. Thus, commonly observed reaction pathways such as oxidation to form oxo-bridged iron(III) dimers are disfavored for $[Fe^{II}(TFPPBr_8)Cl]^-$. Furthermore, the subsequent steps with

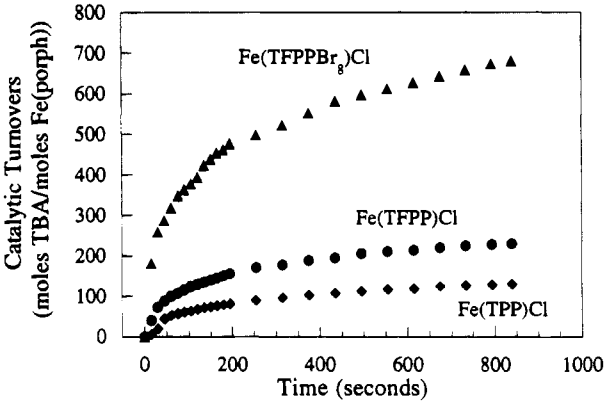

Figure 6. Catalytic decomposition of *tert*-butyl hydroperoxide by iron porphyrins at 23 °C in CH_2Cl_2.

dioxygen and heme to produce a catalytically active high-valent iron–oxo species (as proposed for cytochrome P450) do not occur.[4] Porphyrin systems that do generate ferryl species (*e.g.*, horseradish peroxidase) have iron(III/II) potentials that are typically less than 0 V *vs* NHE, with the iron center generally bonded to electron-donor ligands. Mansuy has noted that electron-withdrawing substituents (*e.g.*, halogens, etc.) decrease the biomimetic-catalytic activity of iron porphyrins.[24] On the other hand, iron porphyrins that perform electron-transfer reactions (excluding oxygen transfer) have iron(III/II) potentials over a wide range (*e.g.*, the potentials of cytochromes range from approximately −170 to 300 mV *vs* NHE).[25]

Although unreactive toward O_2, both $Fe^{III}(TFPPBr_8)Cl$ and $[Fe^{II}(TFPPBr_8)Cl]^-$ efficiently catalyze the decomposition of *tert*-butyl hydroperoxide (TBHP) to *tert*-butyl alcohol and dioxygen. Addition of TBHP to a solution of $Fe^{III}(TFPPBr_8)Cl$ produces copious amounts of dioxygen in a few seconds (Figure 6).[26] High catalytic turnovers are observed within the first few minutes for TBHP decomposition. The TBHP reaction with $Fe^{III}(TFPP)Cl$ or $Fe^{III}(TPP)Cl$ is dramatically slower. The Soret absorption of $Fe^{III}(TFPPBr_8)Cl$ (440 nm) remains essentially unchanged during gas evolution. Addition of TBHP to an electrochemically generated solution of $[Fe^{II}(TFPPBr_8)Cl]^-$ (Soret band at 478 nm) quickly produces the spectral features of the iron(III) state (440 nm) with accompanying gas evolution. Preliminary stopped-flow experiments of TBHP with $[Fe^{II}(TFPPBr_8)Cl]^-$ suggest that the rate constant for iron(II) oxidation is approximately 500 M^{-1} s^{-1}. It is apparent that $Fe(TFPPBr_8)Cl$ can both oxidatively and reductively decompose alkyl hydroperoxides and that the rate-limiting step in alkyl hydroperoxide decomposition is alkyl hydroperoxide oxidation (Scheme 1).

Why are halogenated iron porphyrins such good peroxide decomposition catalysts and, hence, able to catalyze isobutane oxidation? The key appears to be stabilization of lower oxidation states by the electronegative halogen substituents. Peroxide decomposition follows the Haber–Weiss mechanism,[27] where ROOH alternately reduces Fe(III) and oxidizes Fe(II) (Scheme 1); since most iron porphyrin complexes prefer to be

(23) Jayaraj, K.; Gold, A.; Tone, G. E.; Helms, J. H.; Hatfield, W. E. *Inorg. Chem.* **1986**, *25*, 3516–3518.

(24) Lu, W. Y.; Bartoli, J. F.; Battioni, P.; Mansuy, D. *New J. Chem.* **1992**, *16*, 621–628.

(25) Moore, G. R.; Pettigrew, G. W. *Cytochromes c: Evolution, Structure, and Physiochemical Aspects*; Springer-Verlag: Berlin, 1990.

(26) (a) Lyons, Ellis, and co-workers have reported that $Fe^{III}(TFPPCl_8)Cl$ is a highly active catalyst for TBHP decomposition: Lyons, J. E.; Ellis, P. E.; Meyers, H. K.; Wagner, R. W. *J. Catal.* **1993**, *141*, 311–315. (b) The catalytic turnovers reported are based on moles of TBHP decomposition (TBHP → ROH + $^1/_2O_2$) per mole of catalyst. However, reactions such as RO• reacting with ROOH that do not involve the metal also lead to TBHP decomposition.

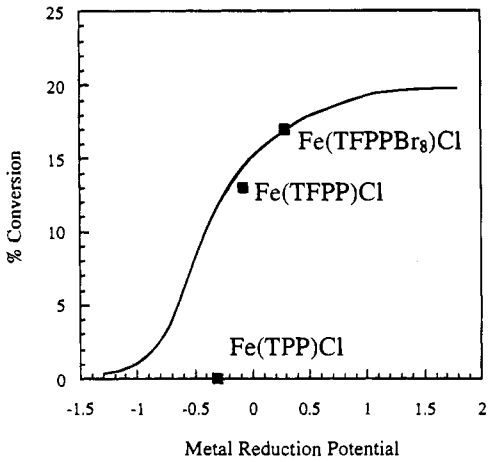

Figure 7. Plot of % conversion of isobutane to *tert*-butanol *vs* iron(III/II) reduction potential (V). The calculated curve is from a radical chain autoxidation model.[6]

in the ferric state, oxidation of the peroxide is generally the slow or rate-determining step. Figure 6 shows the catalytic activity of peroxide decomposition with iron porphyrins. The fully halogenated complex (Fe(TFPPBr$_8$)Cl; 0.31 V *vs* AgCl/Ag) is significantly more active than the other iron porphyrins. Hence acceleration of the oxidation of the peroxide by stabilizing Fe(II) relative to Fe(III) can markedly accelerate the overall catalytic process. Figure 7 shows this correlation in alkane oxygenation activity *vs* Fe(III)/Fe(II) redox potential for Fe(TFPPBr$_8$)Cl/O$_2$ catalyzed reactions.

Our mechanistic findings have implications for future research in this area. What once seemed the obvious goal—a more active catalyst—appears of questionable value for two reasons. First, in the radical chain autoxidation mechanism, the lack of success with lighter alkanes is not primarily due to the lower reactivity of secondary and primary C−H bonds (although that does play a role). Rather it is because the chain termination steps are *much more* efficient for secondary and primary alkyl peroxy radicals (eq 1) than for tertiary (eq 2). This has a severe effect on both activity and selectivity and makes it unlikely that catalysis based on this mechanism can be useful for oxidation of nontertiary centers.

$$2R_2HCOO^{\bullet} \rightarrow R_2HCOH + R_2C{=}O + O_2 \qquad (1)$$

$$2R_3COO^{\bullet} \rightarrow R_3COOCR_3 + O_2 \qquad (2)$$

Second, modeling studies (Figure 7; sigmoidal curve)[6] show that the catalytic process eventually levels off as a result of efficient chain termination steps and that increases in the peroxide decomposition rate (presumably achievable by increasing the redox potential) have little effect. It is apparent that we will need to escape from the radical chain autoxidation realm if we want to extend reactivity to a wide range of alkanes. The obvious direction is to move toward systems (*e.g.*, Ru, Re, Os) that may achieve metal−oxo mechanisms[28] like that proposed by Lyons and Ellis.[2]

Experimental Section

Materials. Zinc(II) tetrakis(pentafluorophenyl)porphyrin (ZnTFPP) was used as received from Porphyrin Products. Methanol, chloroform, acetone, dichloromethane, benzene, pyridine, and hexane were used as received from EM Science. Acetone-d_6, chloroform-d_3, N-bromosuccinimide, *tert*-butyl hydroperoxide (TBHP), and $FeCl_2$ were purchased from Aldrich.

Synthesis. Fe^{III}(TFPPBr$_8$)Cl. Halogenation of the porphyrin macrocycle was performed as previously described.[29] Iron was inserted into the porphyrin using the standard metal-insertion methods with $FeCl_2{\cdot}4H_2O$ or $Fe(OAc)_2$.[30] Crystals of Fe^{III}(TFPPBr$_8$)Cl were obtained from vapor diffusion of hexane in chloroform and used for all subsequent reactions and characterizations: (a) UV−vis (CH_2Cl_2) λ_{max} (log ϵ) 402 (4.91), 442 (4.93), 560 (4.15) nm. (b) Mass spectrum (FAB) M^+ *m/e* 1658 (calcd *m/e*1657). (c) Anal. Calcd for $C_{44}N_4F_{20}Br_8FeCl$: C, 32.6; N, 3.2; Fe, 3.3. Found: C, 32.3; N, 3.2; Fe, 3.8. (d) ^{19}F NMR resonances of the fluorophenyls of Fe^{III}(TFPPBr$_8$)Cl are broad and shifted due to the high-spin iron as observed for Fe^{III}(TFPP)Cl with the ortho (−104.4, −108.0), para (−141.9), and meta (−152.5, −153.3 ppm) resonances downfield of C_6F_5X compounds. The pattern observed is consistent with a five-coordinate paramagnetic metal porphyrin.[29]

Fe^{II}(TFPPBr$_8$)(py)$_2$. Fe^{II}(TFPPBr$_8$)(py)$_2$ was obtained by treating Fe^{III}(TFPPBr$_8$)Cl with excess pyridine for 1 h at room temperature. Crystals of Fe^{II}(TFPPBr$_8$)(py)$_2$ were obtained from vapor diffusion of hexane in chloroform and used for all subsequent reactions and characterizations: (a) UV−vis (CH_2Cl_2) λ_{max} 454, 556, 588 nm. (b) ^{19}F NMR resonances (−138.6 ppm (2F, q, ortho), −152.0 (1F, t, para), −163.1 (2F, m, meta)) of the fluorophenyls of Fe^{II}(TFPPBr$_8$)(py)$_2$ are sharp and similar to the pattern observed for the diamagnetic Zn(TFPPBr$_8$).[29] The ^{19}F NMR spectrum of Fe^{II}(TFPPBr$_8$)(py)$_2$ indicates an axially symmetric coordination structure.

Methods. Electronic absorption spectra were recorded on a HP 8452 diode array spectrometer. ^{19}F-NMR spectra in $CDCl_3$ were recorded on a Bruker AM-500 (tuned down to 470.56 MHz for fluorine detection) instrument and referenced externally to $CFCl_3$ at 0 ppm. Magnetic measurements were performed on a SQUID magnetometer (Quantum Design, MPMS). Electron paramagnetic resonance experiments were made on a Bruker X-band instrument (toluene glass). Cyclic voltammetric experiments on Fe^{III}(TPP)Cl, Fe^{III}(TFPP)Cl, Fe^{III}(TFPPBr$_8$)Cl, and Fe^{II}(TFPPBr$_8$)(py)$_2$ were performed at 25 °C under argon in CH_2Cl_2 with 0.1 M TBAH as the supporting electrolyte (TBAH = tetrabutylammonium hexafluorophosphate). Potentials are versus AgCl/Ag in 1 M KCl. The Fe$^{III/II}$ couple of ferrocene was observed at 0.45 V under these experimental conditions.

Crystal Structure Analysis. Crystals of Fe^{III}(TFPPBr$_8$)Cl and Fe^{II}(TFPPBr$_8$)(py)$_2$ were grown by diffusion of hexane in chloroform. Suitable crystals were mounted in capillaries with silicon grease and centered on a CAD-4 diffractometer (monochromatic Mo Kα radiation). Atomic scattering factors were taken from Cromer and Waber;[31] CRYM,[32] MULTAN,[33] and ORTEP[34] computer programs were used. The CRYM program was used for absorption correction, and no corrections for the presence of extinction were made.

X-ray data for both Fe^{III}(TFPPBr$_8$)Cl and Fe^{II}(TFPPBr$_8$)(py)$_2$ were consistent with either P1 or P$\bar{1}$ as a possible space group. The structures were solved and refined in space group P$\bar{1}$. The iron and bromine atoms in Fe^{III}(TFPPBr$_8$)Cl and Fe^{II}(TFPPBr$_8$)(py)$_2$ were located by MULTAN. The remaining carbon and halogen atoms in both Fe^{III}(TFPPBr$_8$)Cl and Fe^{II}(TFPPBr$_8$)(py)$_2$ were found from successive structure factor-Fourier calculations. In Fe^{II}(TFPPBr$_8$)(py)$_2$ the hydrogens on the pyridines were positioned by calculation with *B* assigned

(27) (a) Sheldon, R. A.; Kochi, J. K. *Metal Catalyzed Oxidations of Organic Compounds*; Academic Press: New York, 1981. (b) Sosnovsky, G.; Rawlinson, D. J. In *Organic Peroxides*; Swern, D., Ed.; Wiley: New York, 1971; pp 153−268.

(28) O-atom donors such as PhIO have been used to generate high-valent iron−oxo complexes to selectively oxidize substrates.[3]

(29) Birnbaum, E. R.; Hodge, J. A.; Grinstaff, M. W.; Schaefer, W. P.; Henling, L.; Labinger, J. A.; Bercaw, J. E.; Gray, H. B. *Inorg. Chem.* **1995**, *34*, 3625−3632.

(30) (a) Adler, A. D.; Longo, F. R.; Kampos, F.; Kim, J. *Inorg. Nucl. Chem.* **1970**, *32*, 2443−2445. (b) Warburg, O.; Negelein, E. *Z. Biochem.* **1932**, 14−32.

(31) Cromer, D. T.; Waber, T. J. *International Tables for X-ray Crystallography;* Kynoch Press: Birmingham, U.K., 1974; Vol. IV, pp 99−101.

(32) Cromer, D. T. *International Tables for X-ray Crystallography;* Kluwer Academic Publishers: Dordrecht, The Netherlands, 1974; Vol. IV, pp 149−151.

(33) Duchamp, D. J. Presented at the Am. Crystallogr. Assoc. Meet., Bozeman, MT, 1964; Paper B14, p 29.

(34) Johnson, C. K. In *Report ORNL-3794*; Oak Ridge National Laboratory: Oak Ridge, TN.

as about 1.1 times U_{eq} of the bonded C atoms, averaged over the three pyridines (two coordinated, and one pyridine solvent molecule in the unit cell).

TBHP Reactivity. Approximately 4 mg of iron porphyrin (Fe(TPP)Cl, Fe(TFPP)Cl, or $Fe^{III}(TFPPBr_8)Cl$) was added to a 25 mL single-neck round-bottom flask that contained 10 mL of TBHP (95%) and 2 mL of methylene chloride (mole ratio of Fe(porph) to TBHP; $1:10^5$). Dioxygen evolution from TBHP was monitored using a graduated buret at 23 °C.

Dioxygen Reactivity. $[Fe^{II}(TFPPBr_8)Cl]^-$ was generated by bulk electrolysis of $Fe^{III}(TFPPBr_8)Cl$ at 0.0 V under argon in CH_2Cl_2 with 0.1 M TBAH as the supporting electrolyte at 25 °C. $[Fe^{II}(TFPPBr_8)Cl]^-$ was transferred to a degassable cuvette under an inert atmosphere. The solution was then purged with dioxygen and monitored by UV−vis spectroscopy.

Acknowledgment. We thank Jim Lyons, Paul Ellis, John Bercaw, Yi Lu, Michael Murphy, Julia Hodge, and Toshi Takeuchi for valuable discussions. Fellowship support from the NIH (M.W.G.) and NDSEG (E.R.B.) is acknowledged. This work was supported by the National Science Foundation, the U.S. Department of Energy, Morgantown Energy Technology Center, and the Sun Co., Inc.

Supporting Information Available: Tables of X-ray crystallographic data for $Fe^{III}(TFPPBr_8)Cl$ and $Fe^{II}(TFPPBr_8)(py)_2$ (27 pages). Ordering information is given on any current masthead page.

IC950089N